J Mater Sci (2015) 50:3371–3382
DOI 10.1007/s10853-015-8888-1

Templated non-hydrolytic synthesis of mesoporous zirconium silicates and their catalytic properties

David Skoda · Ales Styskalik · Zdenek Moravec · Petr Bezdicka · Jiri Pinkas

Received: 21 December 2014 / Accepted: 2 February 2015 / Published online: 13 February 2015

Abstract A novel non-hydrolytic sol–gel (NHSG) synthesis of mesoporous zirconium silicate xerogels is presented. The condensation between silicon acetate, $Si(OAc)_4$, and $Zr(NEt_2)_4$ resulting in acetamide elimination leads to homogeneous zirconium silicate xerogels containing Si–O–Zr linkages. The addition of Pluronic P123 template provides stiff gels that are after template removal by calcination at 500 °C in air converted to stable mesoporous xerogels with wormhole-type pores, high surface area over 500 $m^2\ g^{-1}$, and tetrahedrally coordinated Zr atoms in the framework. The composition and morphology of the xerogels, volatile reaction byproducts, and thermal transformations were followed by elemental analysis, IR spectroscopy, thermal analysis TG-DSC, nitrogen adsorption, ^{13}C and ^{29}Si solid-state NMR spectroscopy, DRUV–Vis spectroscopy, SAXS, and HT powder XRD. These potential catalysts were tested for the Meerwein–Ponndorf–Verley reduction of 4-*tert*-butylcyclohexanone and for aminolysis of styrene oxide with aniline. Resulting reaction systems display good activity and selectivity.

D. Skoda · A. Styskalik · Z. Moravec · J. Pinkas (✉)
Department of Chemistry, Masaryk University, Kotlarska 2, 61137 Brno, Czech Republic
e-mail: jpinkas@chemi.muni.cz

D. Skoda · A. Styskalik · J. Pinkas
CEITEC MU, Masaryk University, Kamenice 735/5, 62500 Brno, Czech Republic

P. Bezdicka
Institute of Inorganic Chemistry, ASCR, 25068 Rez, Czech Republic

Introduction

In recent years, SiO_2–ZrO_2 mixed oxides have attracted much interest for their physicochemical properties, such as high thermal and chemical stability, mechanical strength and surface acidity [1]. Porous materials containing Zr have received considerable attention in heterogeneous catalysis owing to the moderate acidity and unique oxidizing abilities of Zr active species. Zirconia is active in a number of reactions, such as oxidation, hydrogenation of aromatic carboxylic acids [2], Fischer–Tropsch synthesis of alkenes from carbon monoxide and hydrogen over zirconia-supported nickel catalyst [3], CO_2 reforming of CH_4 over nickel catalysts on mesoporous nanocrystalline zirconia support [4], methanol synthesis over zirconia-supported copper catalyst [5], etc. Unfortunately, zirconia could only be prepared with surface areas (SA) lower than 200 $m^2\ g^{-1}$ and its active sites are non-isolated, which limits its applications. The Meerwein–Ponndorf–Verley (MPV) reduction of carbonyl compounds uses secondary alcohols as a hydrogen donor, and the mechanism involves a hydrogen transfer via a six-membered cyclic intermediate with the alcohol and the carbonyl compound both coordinated to the Zr or Hf centers of the catalyst [6]. There is an effort focused on immobilization of MPV reduction catalysts on solid supports. Incorporating Zr ions into the zeolite framework proved to be one of the most promising methods. Zirconium silicates with the structures of MFI [7], MEL [8], AlPO-5 [9], and zeolite beta [10] serve as active catalysts showing very high specific surface area and shape selectivity. However, the narrow pores of these microporous materials restrict their applications to the small substrates. To overcome the pore size limitation, incorporation of Zr into mesoporous silica substrates is considered. For example, some Al and Zr alkoxides or Zr and Hf alkyl complexes have been anchored on amorphous SiO_2, MCM-

41, [11–13], MCM-48 [14], and KIT-6 [15]. Compared with zeolitic zirconium silicates, these Zr-containing mesoporous materials have wider pores and higher SA. Hydrolytic synthesis of a mesoporous Zr-SBA-15 catalyst for the Prins reaction [16] and hydrothermal preparation of mesoporous zirconium silicate by the reaction of $ZrCl_4$ and tetraethoxysilane (TEOS) in the presence of a template, [3-(trimethoxysilyl)propyl]octadecyldimethylammonium chloride, and tetrapropylammonium hydroxide (TPAOH) [17] were reported. Recently, Kore et al. prepared an efficient nanocrystalline zirconium silicate catalyst for the aminolysis, alcoholysis, and hydroamination reactions [18] by a condensation between tetraethoxysilane, propyltriethoxysilane, and zirconium alkoxide in the aqueous solution of TPAOH. A related approach was used in the synthesis of Zr-silicalite-1 with micro-meso-macroporous architecture [19]. Zirconium silicates were also prepared by solvothermal decomposition of a single-source precursor in toluene at 135 °C according to Eq. 1 [20]:

$$\mathrm{Zr}\left[\mathrm{OSi}(\mathrm{O}^t\mathrm{Bu})_3\right]_4 \rightarrow \mathrm{ZrO_2}.4\mathrm{SiO_2} + 12\,\mathrm{CH_2{=}CMe_2} + 6\,\mathrm{H_2O} \quad (1)$$

The metal precursors used in these reactions display hydrolysis rates that are very fast in comparison with TEOS. Therefore, the control of heterocondensation is complicated, and it is necessary to decrease hydrolysis rate of metal precursors. It could be done by modification of the metal precursors by inhibitors, such as inorganic acids or multidentate ligands (carboxylates, β-diketonates, etc.), to tune the reactivity of the metal alkoxides [21] or by prehydrolyzing the precursor having the lowest reactivity [22]. A different approach to overcoming these problems is a non-hydrolytic sol–gel (NHSG) method [23, 24]. In these processes, the networks of M–O–M′ bridges are obtained by condensation between the precursors containing halides or other functional organic groups. Since the NHSG methods do not include the hydrolysis step, the oxygen is provided by other reagents, such as alcohols, ethers, alkoxides, or acetates. Several basic types of reactions were reported for the NHSG preparation of zirconium silicates. Andrianainarivelo et al. synthesized zirconium and titanium silicates by the alkylhalide elimination reaction between isopropoxide and halide functions at 110 °C [25]. The same procedure was used for the preparation of porous SiO_2–ZrO_2 catalysts for Friedel–Crafts alkylation [26]. Another type of non-hydrolytic condensation is the reaction between silicon acetate and metal alkoxides which leads to the formation of Si–O–M bonds and elimination of acetic acid esters as byproducts. The reaction of $Si(OAc)_4$ and $Zr(O^nPr)_4$ in dry toluene was used by Jansen et al. [27].

As we have recently reported, non-hydrolytic acetamide elimination can be successfully used for the synthesis of titanosilicate catalysts [28]. Here, we present results of the application of this novel acetamide elimination principle (Eq. 2) together with the templating effect of triblock copolymer Pluronic 123 to the preparation of mesoporous zirconium silicates and characterization of the obtained xerogels by a variety of instrumental techniques.

$$\mathrm{Si(OC(O)CH_3)_4 + Zr\,(NEt_2)_4 \rightarrow SiO_2{-}ZrO_2} + 4\ \mathrm{Et_2NC(O)CH_3} \quad (2)$$

The obtained xerogels were tested for catalytic MPV reduction of 4-*tert*-butylcyclohexanone and for aminolysis of styrene oxide with aniline.

Experimental

General procedures

All manipulations were performed in a dry nitrogen atmosphere using Schlenk techniques as well as in an M. Braun drybox with both H_2O and O_2 levels below 1 ppm.

Chemicals, such as Pluronic P123 ($EO_{20}PO_{70}EO_{20}$ $M_{av} = 5845$ g mol^{-1}), 4-*tert*-butylcyclohexanol (99 %), 4-*tert*-butylcyclohexanone (99 %), $ZrCl_4$ (99 %), styrene oxide (97 %), aniline and nonane, were purchased from Sigma-Aldrich. $Si(OAc)_4$ and $Zr(NEt_2)_4$ were synthesized according to the published procedures [29, 30]. Toluene and isopropanol were dried by standard methods and distilled before the use. Pluronic P123 was dried under vacuum at 60 °C and dissolved in dry toluene. Syntheses of the xerogels were performed under inert dry N_2 atmosphere according to Eq. 2.

Synthesis of zirconium silicates

Zirconium silicate xerogels synthesized without a template-SiZr1

$Zr(NEt_2)_4$ (1.482 g; 3.903 mmol) was added dropwise with a syringe to a stirred solution of $Si(OAc)_4$ (1.016 g; 3.844 mmol) in toluene (40 cm^3). After the addition, the color of the mixture changed to light green–yellow. The reaction mixture was heated at 80 °C. The reaction was stopped after 168 h, the volatile byproducts were separated in vacuo, and the yellow powder was dried under vacuum for 48 h. Yield 1.495 g, theor. 0.715 g; DC = 57 %.

IR spectra (KBr, cm^{-1}): 514 vw, 585 vw, 617 vw, 655 vw, 768 w, 790 w (ν Si–O–Si), 968 s (ν Si–O–Zr), 1011 very strong (vs) (ν Si–O–Si), 1164 w, 1208 vw (ν Si–O–Si), 1281 m (δ CH_2), 1311 w, 1363 m (δ CH), 1378 m (δ CH_3), 1456 s (ν COO), 1506 s, 1577 vs (ν COO), 1636 m

(ν CO), 2876 w (ν CH), 2933 w (ν CH), 2973 m (ν CH), 3420 vw (ν NH).

GC–MS of byproducts (SiZr1): 0.57 min (diethylamine), $m/z = 73$, 58, 44, 30; 3.57 min (diethylacetamide), $m/z = 115$, 100, 86, 72, 58, 44, 43.

Zirconium silicate xerogel synthesized with the Pluronic P123 template-SiZrP4

$Zr(NEt_2)_4$ (1.756 g; 4.625 mmol) was added dropwise with a syringe to a stirred solution of $Si(OAc)_4$ (1.581 g; 5.980 mmol) and Pluronic P123 (1.58 g; 0.270 mmol) in toluene (40 cm^3). After the addition, the color of the mixture changed to light green-yellow. The reaction mixture was heated to 80 °C. After 12 h, a transparent light yellow stiff gel was formed. The reaction was stopped after 168 h, the volatile byproducts were separated in vacuo, and the solid product (yellow gel) was dried under vacuum for 48 h. Yield 3.235 g, theor. 2.513 g; DC = 74 %.

IR spectrum ATR, 586 vw, 614 vw, 653 w, 769 vw, 792 w (ν Si–O–Si), 870 w (δ CH), 964 s (ν Si–O − Zr), 1009 vs (ν Si–O–Si), 1049 vs (ν Si–O–Si), 1092 vs (ν δ C–O–C), 1208 w (ν Si–O–Si), 1247 w (ν CO), 1282 w (δ CH_2), 1373 m (δ CH_3), 1451 s (ν COO), 1504 s (ν COO), 1572 s (ν COO), 1637 m (ν CO), 1738 w (ν COO), 2868 s (ν CH), 2930 m (ν CH), 2970 m (ν CH).

GC–MS of byproducts: 3.58 min (diethylacetamide), $m/z = 115$, 100, 72, 58, 44.

The xerogels were calcined in air at 500 °C for 3 h. Calcined samples were kept in the vial flasks. To identify a gaseous pyrolysis product, xerogel was heated in DIP crucible and MS spectra were collected up to 450 °C.

Catalytic reactions

Calcined zirconium silicate catalysts were degassed before the reaction under vacuum at 115 °C for 20 min. The MPV reduction [17] of 4-*tert*-butylcyclohexanone was carried out in a 50 cm^3 round-bottomed Schlenk flask equipped with a reflux condenser connected to a N_2 source. The reaction mixture containing calcined zirconium silicate xerogel catalyst (100 mg), 4-*tert*-butylcyclohexanone (500 mg, 3.54 mmol), and dry 2-propanol (15 cm^3, 196 mmol) was stirred and refluxed at 115 °C for 4 h. The products were analyzed by GC–MS method using 0.100 cm^3 of nonane as an internal standard. To investigate Zr leaching, 100 mg of the catalyst was refluxed in 15 cm^3 of 2-propanol at 115 °C for 4 h. After filtering off the catalyst powder, the filtrate was tested for the MPV reduction of 4-*tert*-butylcyclohexanone. The reusability of catalyst was tested after washing of the used catalyst with 2-propanol.

Aminolysis of styrene oxide [18] was performed in a 25 cm^3 round-bottomed Schlenk flask connected to a N_2 source. The reaction mixture consisted of 25 mg of calcined zirconium silicate xerogel, 5 cm^3 of dry toluene, 0.456 cm^3 (5.00 mmol) of aniline, 0.587 cm^3 (5.00 mmol) of styrene oxide, and 0.100 cm^3 of nonane as an internal standard. This reaction mixture was heated at 50 °C for 2 h. The reusability of catalyst was studied after washing the used catalyst with toluene and CH_2Cl_2. Catalytic products were analyzed by GC–MS method and ^{1}H NMR spectroscopy.

Characterization

IR spectra were recorded on Bruker Tensor 27 FTIR (KBr pellets) and Bruker Alpha–Platinum ATR spectrometers. GC–MS measurements were performed on a mass spectrometer TSQ Quantum XLS coupled with a gas chromatograph Trace GC Ultra by Thermo Scientific. The gas chromatograph was equipped with a TS-SQC column (length 15 m, diameter 0.25 mm, and film thickness 0.25 μm) using a temperature program: 50 °C (0 min), 5 °C min^{-1} to 80 °C, 15 °C min^{-1} to 120 °C, 35 °C min^{-1} to 200 °C, at this temperature for 0.5 min. Mode injection split, injector temperature, the interface temperature, and detector temperature were all set to 200 °C. The column pressure was 31.5 kPa and the ionization energy was 70 eV. Direct insertion probe (DIP) MS measurements were performed at 50 °C min^{-1} from 30 to 450 °C and with ionization energy of 44 eV. For liquid phase ^{1}H NMR measurements, a Bruker Avance DRX 300 MHz spectrometer was used. Solid-state NMR spectra were measured on a Bruker Avance III 700 MHz spectrometer with a MAS DVT 700S4 BL4 N–P/H probe and on a Bruker Avance III 500 MHz spectrometer with a MAS VTN 500SB BL4 N–P/F–H probe. High-temperature PXRD diffractograms were recorded on an X'PertPRO diffractometer equipped with a $Co_{K\alpha}$ X-ray tube and a HTK 16 high-temperature chamber (Anton Paar, Graz, Austria) with a Pt holder. Samples were measured from 500 to 1200 °C in 50 °C increments. The sample was held during scanning at a constant temperature for 12 min. Nitrogen adsorption/desorption experiments were performed at 77 K on a Quantachrome Autosorb-1MP porosimeter. SA and total pore volumes (V_{tot} at $p/p_0 = 0.98$) were determined by volumetric technique [31, 32]. Prior to the measurements, the samples were degassed at 100 °C for at least 24 h until the outgas rate was less than 0.4 Pa min^{-1}. The adsorption–desorption isotherms were measured for each sample at least three times. The specific surface area was determined by the multipoint BET method with at least five data points with relative pressures between 0.05 and 0.30. Micropore volumes (V_{micro}) were established by a t-plot method [31, 32]. Thermal analysis (TG/DSC) was performed

on a Netzsch STA 449C Jupiter apparatus in the stream of air (70 cm^3 min^{-1}) with a temperature gradient of 5 °C min^{-1} up to 1000 °C, in a Pt crucible. The DRUV spectra were recorded on an Agilent CARY 5000 spectrometer with a Harrick Praying Mantis attachment. Zirconium contents were determined on an ICP optical emission spectrometer iCAP 6500 Duo (Thermo, UK) equipped with a solid-state generator with a frequency of 27.12 MHz and a maximum power input 1350 W. The measurements were performed at 327.3, 339.1, and 343.8 nm. Transmission electron microscopy (TEM) was carried out on a JEOL JEM 3010 microscope operated at 300 kV (LaB_6 cathode, point resolution 1.7 Å) with an Oxford Instruments Energy Dispersive X-ray (EDX) detector attached. SAXS measurements were performed on Rigaku BioSAXS 1000 at a wavelength of 1.5408 Å. Studies of surface acidity were performed on air-calcined xerogels exposed for 30 min to pyridine vapors under static vacuum.

In reactions without template, the yield of the product as well as the mass of starting precursors was precisely weighed to allow gravimetric estimation of the degree of condensation, DC = $100(n_{total}-n_{residual})/n_{total}$, where n_{total} is the molar amount of organic groups in the starting materials and $n_{residual}$ is molar amount of residual organic groups in the xerogel computed from the difference of theoretical and experimental yield. As the condensation reactions were never quantitative, DC represents the relative difference between the maximum theoretical loss of $Et_2NC(O)CH_3$ (Eq. 2) in comparison to what is experimentally observed. This difference also defines the number of acetoxy groups on silicon and diethylamide groups on zirconium that are left in the matrix.

Results and discussion

Zirconium silicate xerogels were synthesized by a novel acetamide elimination according to Eq. 2 from $Si(OAc)_4$ and $Zr(NEt_2)_4$ precursors. The equation represents a complete condensation of the Si–O–Zr network and quantitative elimination of diethylacetamide. However, under experimental conditions, the condensation is incomplete (Scheme 1), and DC for reactions without template were 57 %.

The reaction parameters are summarized in Table 1. The NHSG reactions produced yellowish precipitate, which was dried under vacuum for 48 h to form yellow powders. The surface area of the prepared xerogels was very low so an improvement was achieved by addition of a templating agent Pluronic P123.

The transparent light yellow stiff gels were prepared with Pluronic P123 and then calcined in air at 500 °C for 3 h to eliminate residual organic groups and the template from the pores. Resulting SA were substantially improved and pore sizes corresponded to mesoporous region (see below). The reactions were performed with various molar Si/Zr ratios. The non-hydrolytic condensation between $Si(OAc)_4$ and $Zr(NEt_2)_4$ proceeds with the formation of Si–O–Zr bonds and release of diethylacetamide which was confirmed as a condensation byproduct by GC–MS analysis of the volatiles separated from the reaction mixture. In the case of samples with a lower content of zirconium (SiZrP1, SiZrP2, SiZrP3), acetic acid anhydride and acetic acid were found in the chromatogram. These byproducts arise from the homocondensation of acetoxy species and from the reaction with the –OH groups of the Pluronic template.

The presence of residual organic groups in dried xerogels was confirmed by FTIR spectroscopy. Absorption bands (Fig. 1) were attributed to vibrations of acetate (1451, 1577, 1734 cm^{-1}), $-NEt_2$ (1282, 1373, 2930, 2970 cm^{-1}) [33], and Pluronic P123 C–O–C (1092–1102 cm^{-1}) moieties [34]. The difference between symmetric and asymmetric (1451, 1577 cm^{-1}) carboxylate vibrational bands is 120–130 cm^{-1} and according to Deacon–Phillips rules, it is indicative of the bidentate bridging

Scheme 1 Formation of zirconium silicate network

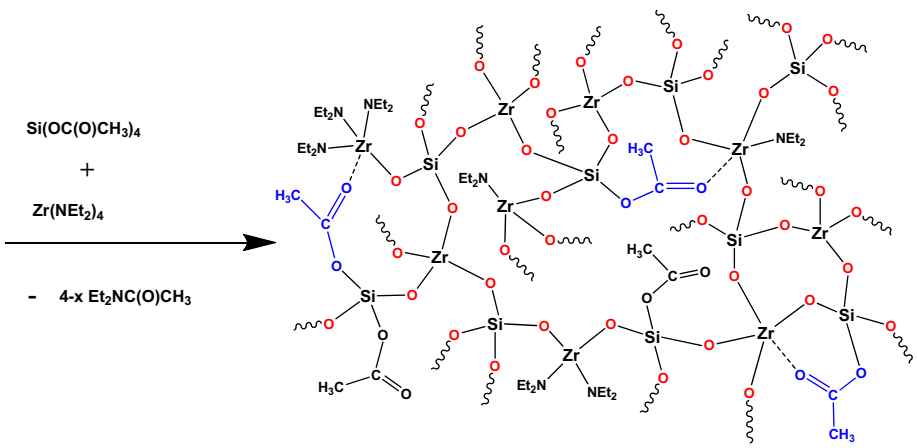

Table 1 NHSG reaction parameters

Sample	$Si(OAc)_4$ n_{Si} (mmol)	$Zr(NEt_2)_4$ n_{Zr} (mmol)	P123 n (mmol)	Nominal[a] mol% Zr
SiZr1	3.845	3.903	–	50.4
SiZrP1	6.486	0.524	0.337	7.5
SiZrP2	5.937	1.709	0.270	22.4
SiZrP3	5.737	2.776	0.270	32.6
SiZrP4	5.983	4.624	0.270	43.6

[a] $Zr_{mol\ \%} = n_{Zr}/(n_{Zr} + n_{Si}) \times 100\ \%$

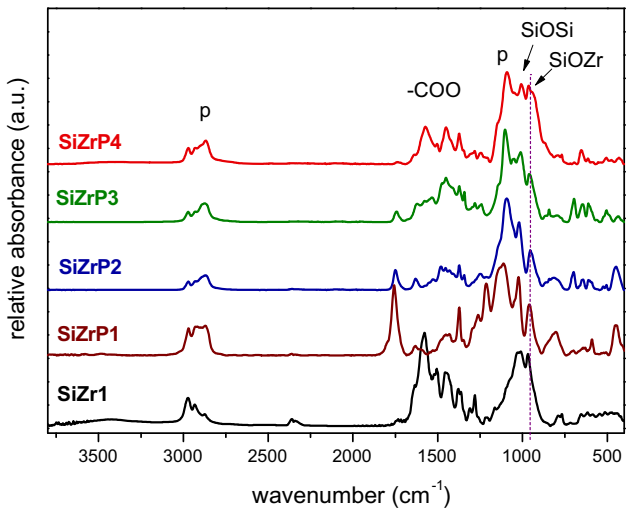

Fig. 1 IR spectra of dried zirconium silicate xerogels. Characteristic vibrational bands are attributed to Si–O–Zr, Si–O–Si, –COO bonds and template fragments (labeled with the letter p). Samples SiZrP2, SiZrP3, and SiZrP4 were measured by the ATR technique

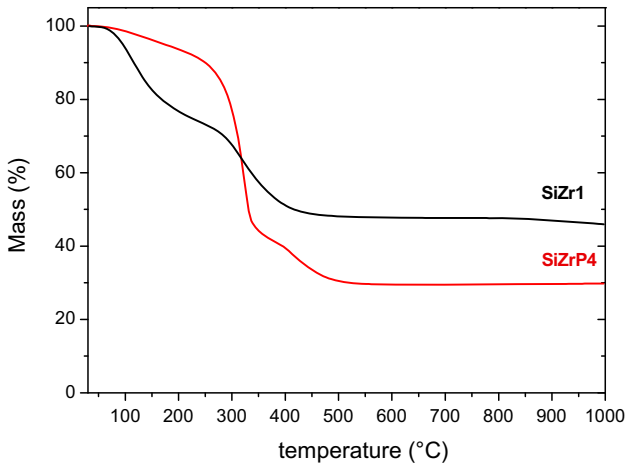

Fig. 2 Thermogravimetric analysis of zirconium silicate xerogels synthesized without (*Black*, SiZr1) and with (*Red*, SiZrP4) the template

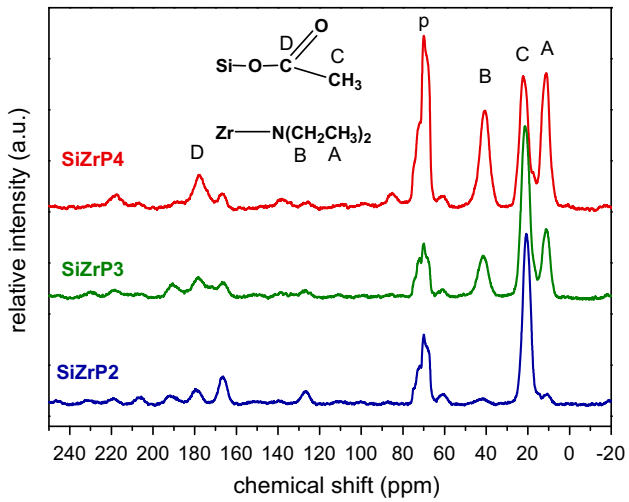

Fig. 3 ^{13}C CPMAS NMR spectra of dried zirconium silicate xerogels prepared with the template

mode on the metal center [35, 36], while the vibrational band at 1734 cm^{-1} characterizes the monodentate acetate groups. Intensity of this band increases with the decrease of Zr content as there are fewer possibilities for the acetates to coordinate through their second oxygen atom. A vibrational band related to Si–O–Zr bridges is observed at 964 cm^{-1} (Fig. 1). This band indicates introduction of Zr^{4+} species in the silicate matrix by the heterocondensation reaction [25, 37–39]. Its increasing relative intensity correlates with higher Zr content in the series of samples. The Si–O–Si linkages (Fig. 1) are represented by absorption bands at 792 (ν_{sym} Si–O–Si), 1009 (ν_{asym} Si–O–Si), 1208 cm^{-1} (ν_{asym} Si–O–Si). These bonds are probably formed by homocondensation in the sol–gel system, where the acetate groups could be activated by coordination to the zirconium atoms (Scheme 1). Anhydrous conditions of the NHSG reactions are reflected in the absence of OH vibrations at 3100–3900 cm^{-1}.

Thermal behavior of the synthesized xerogels was studied by TG/DSC analysis. Mass losses during calcination are attributed to oxidation of the residual organic groups in xerogel and Pluronic P123 template. These species are completely burned away at 500 °C (Fig. 2). The residual mass of the SiZr1 sample (Fig. 2) after TG/DSC analysis (45.9 % at 1000 °C) corresponds with the theoretical yield of oxidic $ZrSiO_4$ material (47.8 %). In the case of the sample prepared with the template (SiZrP4), the theoretical yield of oxidic $ZrSiO_4$ material is 30.1 % of dried product. This number is in a good agreement with the residual mass after TG/DSC (29.8 % at 1000 °C). The gaseous products released during the heating of samples prepared with the template were identified by DIP MS measurement. Further condensation of residual unreacted –OAc and $–NEt_2$ groups leads to release of diethylacetamide during calcination from 80 to 330 °C ($m/z = 115$), while the fragments

$(C_3H_5O)_m{\cdot}(C_2H_3O)_n$ of Pluronic P123 are observed at higher temperatures 335–450 °C.

Solid-state NMR spectroscopy was employed for a deeper characterization of internal xerogel structure. ^{13}C CPMAS NMR spectra of dried xerogels (Fig. 3) display resonances corresponding to residual acetate (CH_3: 22, COO: 178, 167 ppm) and diethylamido (CH_3: 12 ppm, CH_2: 41 ppm) groups. Two signals for the COO moieties are in concert with the presence of bidentate (178 ppm) and monodentate (167 ppm) coordination modes of acetates. The resonances with the chemical shifts of 69 and 72 ppm are assigned to Pluronic P123 (CH_2 and CH) carbons. The CH_3 resonance of the PPO part (expected at 19 ppm) is overlapped by the CH_3 signals of diethylamido groups. The samples with the decreasing Zr loading exhibit the same resonances but the intensities of diethylamido and bidentate acetoxy groups are progressively decreased.

The ^{29}Si CPMAS NMR spectra of the dried xerogels give us information on the homogeneity and structure of the zirconium silicate networks. With reference to silica SiO_2 (Q^4) (–110 ppm) [40], a shift to a lower field was observed for the zirconium silicate resonances. According to Sindorf and Maciel [41], such shift corresponds to Q^3 $(SiO)_3Si(OH)$ and Q^2 $(SiO)_2Si(OH)_2$ sites. However, in our NHSG approach there are no OH groups present in the xerogels as confirmed by the IR spectra (Fig. 1). Therefore, this shift is caused by the incorporation of Zr atoms into the silica framework. Indeed, the ^{29}Si NMR chemical shift of the $Si(OSi)_{4-x}(OZr)_x$ tetrahedra depends on the number of zirconium second neighbors (x). Roughly, each substitution of Si for Zr leads to a low-field shift of about 5–8 ppm [26]. As shown here, ^{29}Si CPMAS NMR spectra (Fig. 4) display broad signals representing $Si(OSi)_4$, $Si(OSi)_3(OZr)$, $Si(OSi)_2(OZr)_2$, and $Si(OSi)(OZr)_3$ silicon environments. The resonances are shifted depending on the number of Zr atoms attached to the SiO_4 center. The samples with the highest loading of Zr (SiZr1, SiZrP4) are composed mostly of the $Si(OSi)_3(OZr)$ (–96 ppm), $Si(OSi)_2(OZr)_2$ (–89 ppm), and $Si(OSi)(OZr)_3$ (–79 ppm) sites. Xerogels with the lower Zr loading (SiOZrP2, SiOZrP3) are represented by $Si(OSi)_3(OZr)$ (–96 ppm) and $Si(OSi)_4$ (–110 ppm) species.

A comparison with the ^{29}Si CPMAS NMR spectrum of a calcined sample (Fig. 5) reveals that there is no shift to SiO_2 species on calcination and observed signals at –96 and –89 ppm are attributed to $Si(OSi)_3(OZr)$ and $Si(OSi)_2(OZr)_2$, respectively.

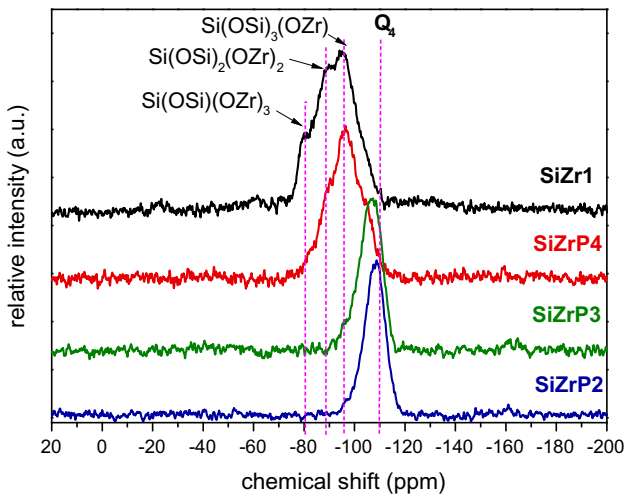

Fig. 4 ^{29}Si CPMAS NMR spectra of dried zirconium silicate xerogels

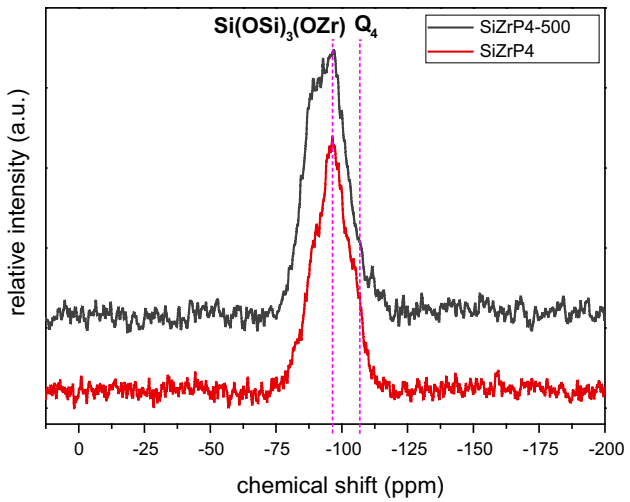

Fig. 5 ^{29}Si CPMAS NMR spectra of calcined (*black*, *top*) and dried (*red*, *bottom*) zirconium silicate (43.6 mol % of Zr) prepared with the template

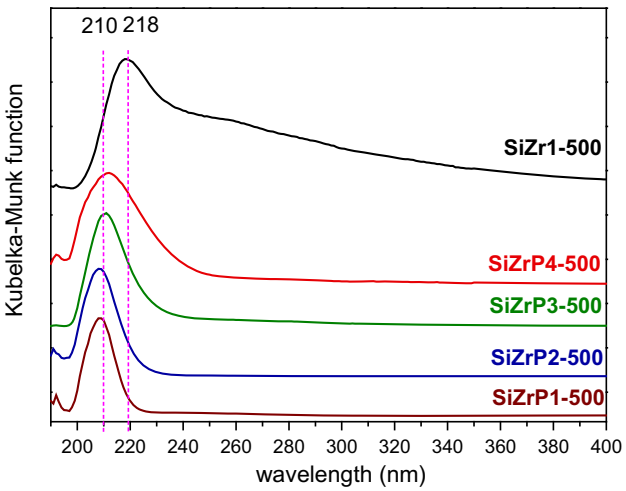

Fig. 6 DRUV-Vis spectra of zirconium silicate xerogels calcined in air at 500 °C

Table 2 Surface areas and porosity parameters of calcined xerogels

Sample	Nominal[a] mol% Zr	ICP mol% Zr	SA BET ($m^2\ g^{-1}$)	d (nm)	V_{tot} ($cm^3\ g^{-1}$)
SiZr1-500	50.4	49.2	10	–	–
SiZrP1-500	7.5	5.1	570	4.3	0.62
SiZrP2-500	22.4	23.2	326	7.7	0.60
SiZrP3-500	32.6	33.5	308	7.2	0.58
SiZrP4-500	43.6	44.4	534	3.1	0.41

[a] $Zr_{mol\%} = n_{Zr}/(n_{Zr} + n_{Si}) \times 100\ \%$

Another effective and sensitive method to study incorporation and coordination of zirconium atoms is the DRUV-Vis spectroscopy. Tetrahedrally coordinated Zr atoms in the xerogel network are the catalytically active sites [42]. The absorption band around 205–215 nm in Zr-containing mesoporous silicas is attributed to the ligand-to-metal charge transfer (LMCT) from O^{2-} to an isolated Zr^{4+} ion in a tetrahedral configuration [14, 19, 43, 44]. In the DRUV-Vis spectra of the calcined samples synthesized with Pluronic P123 (Fig. 6), there are absorption bands with maxima at 208–212 nm which point to the presence of Zr atoms in tetrahedral coordination. The absorption band at 218 nm with a tail at higher wavelengths observed in the spectrum of the sample synthesized without template could be assigned to small ZrO_2 clusters with Zr in higher coordination numbers.

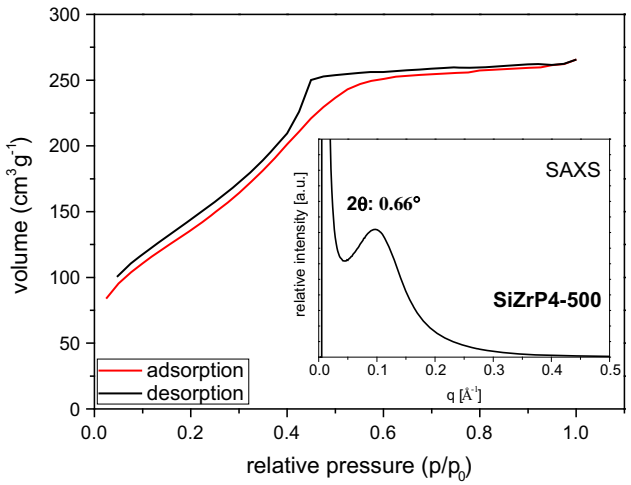

Fig. 7 N_2 adsorption/desorption isotherm and SAXS pattern of the calcined sample SiZrP4-500

Another crucial condition for the catalytic efficiency of these materials is their porosity and large surface area. With the addition of template, we are able to synthesize materials with the mesoporous character after calcination at 500 °C. SA of calcined xerogels are summarized in Table 2. Nitrogen adsorption/desorption isotherms belong to type IV and display hysteresis H2 which is a characteristic for mesoporous materials (Fig. 7) [31, 32]. An isotherm of SiZrP4-500 shows the shape that is indicative of the materials with the framework-confined mesoporosity containing "wormhole-like" pores [20, 45, 46]. This assumption can be confirmed by the TEM experiments (Fig. 8) which reveal "wormhole-like" morphology. Moreover, SAXS analysis shows a diffraction line at 0.66° 2θ which can be assigned to the mesoscopic-ordered structure of zirconium silicate framework with the d spacing of 6.6 nm [45, 46].

According to the BET analysis, the SA of the samples are in the range of 308–570 $m^2\ g^{-1}$. The BJH method shows narrow pore size distributions in Fig. 9 with the diameters characteristic for mesoporous materials [47, 48].

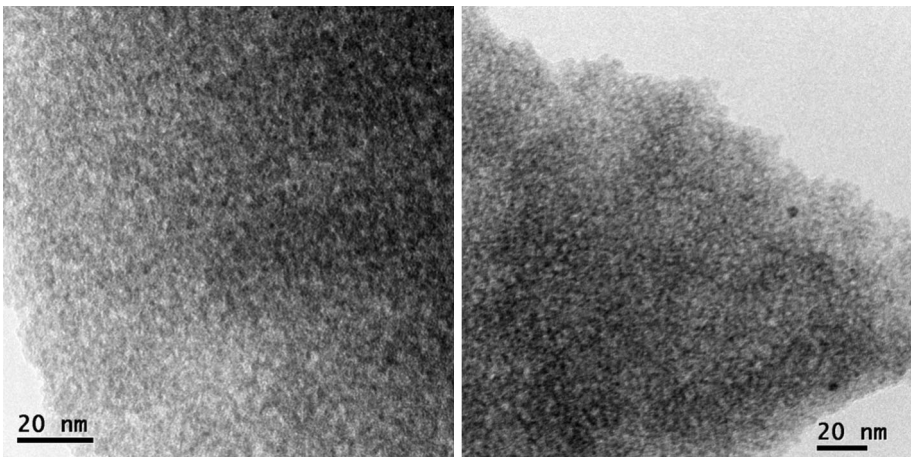

Fig. 8 TEM pictures of the sample SiZrP4-500 prepared with Pluronic P123 template

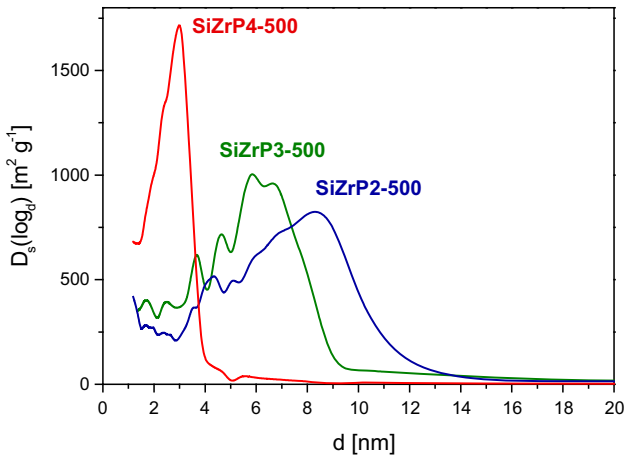

Fig. 9 BJH pore size distributions of calcined zirconium silicate xerogels synthesized with a template determined from the desorption branch

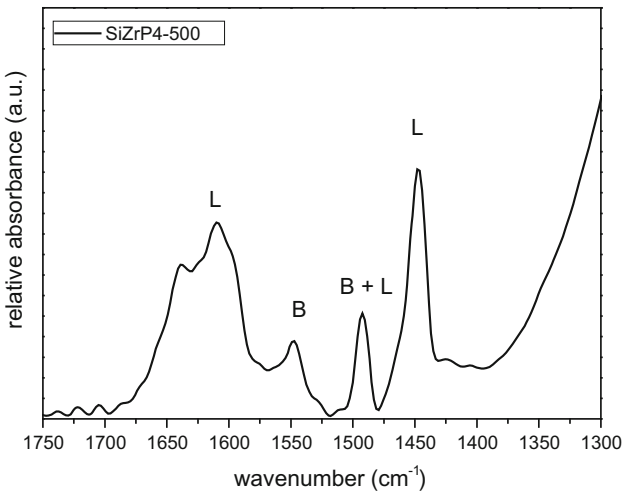

Fig. 10 IR spectrum of xerogel SiZrP4-500 after pyridine adsorption, vibrational bands are attributed to Lewis (L) and Brønsted (B) acid sites

No significant dependence of the porosity on the Zr content was observed. Calcined xerogels synthesized without a template are almost nonporous (<10 m^2 g^{-1}).

The surface acidity of the air-calcined xerogels was studied by pyridine adsorption. The IR spectra of the pyridine-treated samples display weak absorption bands at 1448, 1491, 1547, and 1610 cm^{-1} (Fig. 10). The absorption bands at 1448 and 1610 cm^{-1} are attributed to pyridine molecules coordinated to Lewis acid sites arising from incorporation of Zr into the silica framework [49]. A combination of Lewis and Brønsted (coordinated pyridine and pyridinium ion, respectively) sites is associated with the band at 1491 cm^{-1}. Exclusively Brønsted acidic sites are characterized by the absorption band at 1547 cm^{-1} [16, 17, 44].

HT PXRD technique was employed for the examination of crystallization behavior, resulting phases, and their crystallization temperatures. It was observed that xerogels are amorphous up to 850 °C and in the case of a sample with the lowest Zr loading even up to 1050 °C. Diffractograms (Fig. 11) of the calcined xerogels show diffraction lines corresponding to the tetragonal ZrO_2 phase (PDF 42-1164) with a crystallization temperature of 900 °C. The sample with 43.6 mol% of Zr synthesized with Pluronic P123 exhibits diffraction lines of zircon ($ZrSiO_4$, PDF 81-0590). Crystallization of this phase takes place at 1100 °C and confirms the high homogeneity of Zr and Si mixing on the atomic level in the xerogel. Weak diffraction lines of cristobalite SiO_2 (PDF 27-605) were observed in the diffractogram of the sample with the lowest Zr (7.5 mol%) content. In this case, crystallization of ZrO_2 starts at 1050 °C, and SiO_2 diffraction lines appear at 1150 °C.

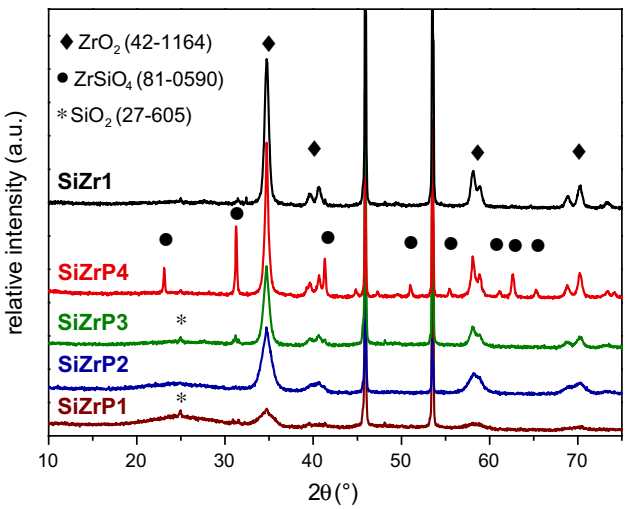

Fig. 11 PXRD difractograms of zirconium silicate xerogels recorded at 1200 °C under air, diffraction lines at 45.9 and 53.5 2θ (°) correspond to the Pt sample holder

Catalytic studies

Catalytic activities of synthesized xerogels were tested in two types of model reactions. At first, the MPV reduction of 4-*tert*-butylcyclohexanone in 2-propanol was investigated [17, 50] with 100 mg of calcined zirconium silicate xerogels as catalysts. The yields of catalytic products were determined by GC–MS analysis with the use of nonane as an internal standard. The only two resulting products of reaction were cis-(ret.time 7.2 min) and trans-4-*tert*-butylcyclohexanol (ret.time 7.5 min), the latter as the major product. Catalytic yields are summarized in Table 3.

Table 3 Results of MPV catalytic reduction of 4-*tert*-butylcyclohexanone, conversions and selectivities

Sample	ICP mol% Zr	SA BET (m^2 g^{-1})	*d* (nm)	Conversion (mol%)[a]	Selectivity (%)	
					cis	*trans*
SiZr1-500	49.2	10	–	0.5	–	–
SiZrP1-500	5.1	570	4.3	5.1	7.8	92.5
SiZrP2-500	23.2	326	7.7	29.0	12.6	87.4
SiZrP3-500	33.5	308	7.2	51.4	10.4	89.6
SiZrP4-500	44.4	534	3.1	54.3	10.5	89.5

[a] to 4-*tert*-butylcyclohexanol, after 4 h

Table 4 MPV reaction parameters and comparison of the 4-*tert*-butylcyclohexanone conversion with different Si/Zr catalysts

Catalyst	Si/Zr ratio	Zr in catalyst (mmol)	SA BET (m^2 g^{-1})	*t* (h)	Cyclohexanone conversion (%)	TOF[a]
SiZrP3-500	2	0.35	308	4	51.4	1.24
SiZrP4-500	1.2	0.43	534	4	54.3	1.06
SiZrP4-500	1.2	0.43	534	14	81.3	0.45
meso-Zr-MFI (150) [17]	196	0.008	454	10	48.0	7.40
meso-Zr-MFI (100) [17]	133	0.012	460	10	84.7	8.90
Zr75 [10]	84	–	499	1	97.3	–
Zr100 [10]	107	–	470	1	95.2	–
Zr200 [10]	194	–	474	1	72.8	-

[a] *TOF* turnover frequency, [mmol $mmol^{-1}$ h^{-1}]

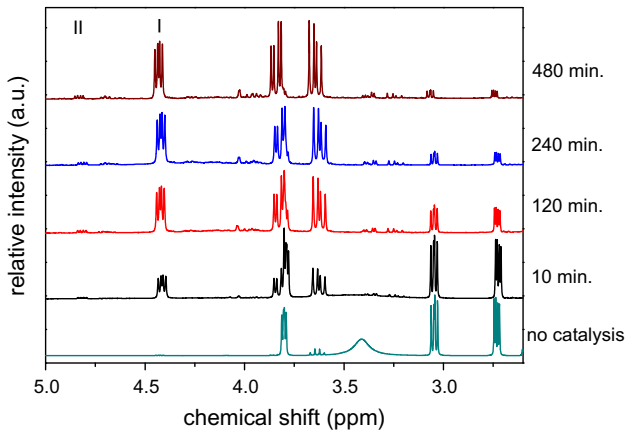

Fig. 12 ^{1}H NMR spectra of catalytic reaction mixtures during catalysis

To establish that Zr active sites are not leached during the reaction, 100 mg of catalyst was refluxed in 2-propanol (15 cm^3) for 4 h. After filtering off the catalyst powder, the filtrate was tested for the MPV reduction of 4-*tert*-butylcyclohexanone. No reaction products were obtained. Also, the ICP analysis of the filtrate confirmed that no leaching of Zr occurs. The highest conversion of 4-*tert*-butylcyclohexanone (54.3 %) was observed in the case of xerogel SiZrP4-500 (Table 3). A comparison between our zirconium silicate catalysts and the catalysts reported by other groups is given in Table 4.

The second reaction tested was aminolysis of styrene oxide by aniline using 25 mg of calcined zirconium silicate as catalyst at 50 °C [18]. The ^{1}H NMR spectra of the reaction mixture display resonances attributed to solvent, substrates (2.7, 3.0, 3.4, 3.8 ppm), and two products: 2-phenyl-2-(phenylamino)ethanol (**I**) and 1-phenyl-2-(phenylamino)ethanol) (**II**) (Fig. 12). These products were also confirmed by GC–MS technique.

Catalytic yields are summarized in Table 5. Two calcined samples of zirconium silicate xerogels were used, SiZrP4 and SiZrP2, with 43.6 and 22.4 mol% of Zr, respectively. Both catalysts exhibit high activity in aminolysis of styrene oxide with aniline which yielded the major product **I** and **II** as a minor product. The highest yield of the catalytic reaction after 2 h (96 %) was observed for the SiZrP2 catalyst.

Dependence of the styrene oxide conversion on the reaction time was studied with SiZrP4-500 and SiZrP2-500 catalysts (Fig. 13). For the catalyst SiZrP4-500, it reached 39 % after 10 min and 94 % after 8 h, while for the catalyst SiZrP2-500 it was 48 % after only 5 min (TOF 436 mmol $mmol^{-1}$ h^{-1}). This higher catalytic activity of SiZrP2-500 as compared to SiZrP4-500 could be ascribed to a higher pore diameter and to a larger pore volume of the former catalyst. According to the DRUV-Vis spectra (Fig. 6), the xerogel SiZrP2-500 also contains a higher amount of tetrahedrally coordinated Zr atoms. Reusability of the SiZrP4-500 catalyst was tested after separation by

Table 5 Styrene oxide aminolysis, reaction parameters, catalytic yields, and comparison with other Si/Zr catalysts

Sample	ICP mol% Zr	Zr in catalyst (mmol)	SA BET (m^2 g^{-1})	*d* (nm)	*t* (min)	Conversion (%)	Selectivity (%)		TOF[a]
							I	II	
SiZrP2-500	23.2	0.066	326	7.7	5	48	93.8	6.2	436
SiZrP2-500					10	58	94.6	5.4	264
SiZrP2-500					120	96	95.8	4.2	36
SiZrP4-500	44.4	0.109	534	3.1	10	39	94.5	5.5	107
SiZrP4-500					120	73	94.9	5.1	17
Zr-Nano(PrTES) [18]	57.8[b]	0.009	565	–	5	75	97.0	3.0	6360

[18] conditions: 25 mg of catalyst, 5 mmol of substrates, 3 cm^3 of toluene, 45 °C

[a] turnover frequency [mmol $mmol^{-1}$ h^{-1}]

[b] Si/Zr mol ratio

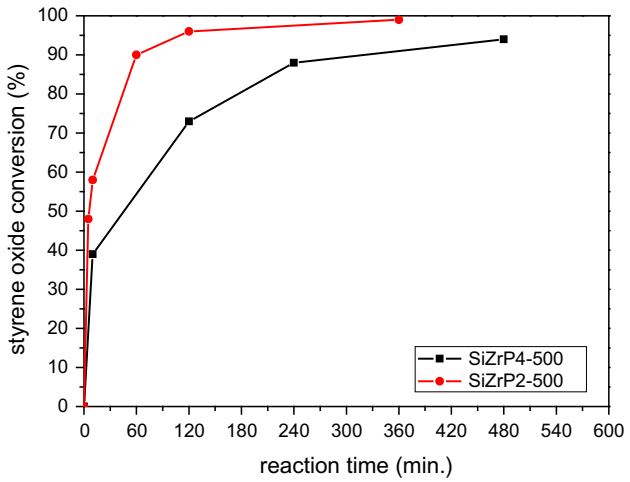

Fig. 13 Catalytic conversions of styrene oxide

centrifugation and washing with toluene and CH_2Cl_2. After drying the catalyst at 120 °C under vacuum, the second catalytic test was performed. The conversion after 2 h reached 69 % which was only slightly less than in the first run (73 %).

Conclusions

In this paper, the novel and effective non-hydrolytic synthesis for mesoporous zirconium silicates with high catalytic performance is presented. Mesoporous xerogels were successfully prepared by acetamide elimination reaction in toluene. This efficient approach allows us to prepare homogeneous mixed oxide materials with the Si–O–Zr linkages, while the volatile diethylacetamide is released as the condensation byproduct. With the addition of Pluronic P123 as a templating agent, we obtained mesoporous materials stable upon calcination at elevated temperatures. The framework-confined mesoporosity was observed in nitrogen adsorption/desorption experiments and TEM micrographs reveal "wormhole-like" morphology characterized by a low-angle diffraction in SAXS. Frameworks of these xerogels contain a high amount of tetrahedrally coordinated Zr atoms that represent catalytically active sites possessing Lewis acidity. All samples were tested for catalytic performance in the MPV reduction of 4-*tert*-butylcyclohexanone and in the aminolysis of styrene oxide. We found that our zirconium silicate xerogels are efficient catalysts for both of these model reactions. The highest conversion of 4-*tert*-butylcyclohexanone (54.3 %) was obtained with the SiZrP4-500 catalyst. In the case of styrene oxide aminolysis, our catalysts exhibit a very high catalytic activity. The best results were achieved for the sample SiZrP2-500 with 23 mol% of Zr. The yield of the catalytic products was 48 % after 5 min with the TOF of 434 mmol $mmol^{-1}$ h^{-1}. The conversion after 2 h reached 96 %.

Acknowledgements Authors thank the project CEITEC—Central European Institute of Technology CZ.1.05/1.1.00/02.0068 and KONTAKT II LH11028 for the financial assistance. A.S. thanks the Brno City Municipality for Brno Ph.D. Talent Scholarship. Authors thank L. Simonikova and Dr. K. Novotny for ICP-OES analyses, L. Krauskova for DRUV-Vis spectra measurements, Dr. M. Klementova for TEM analyses, and Dr. T. Klumpler (Single Crystal X-ray Diffraction Core Facility CEITEC) for the SAXS measurements.

References

1. Rodríguez Avendaño RG, De Los Reyes JA, Viveros T, Montoya De La Fuente JA (2009) Synthesis and characterization of mesoporous materials: silica–zirconia and silica–titania. Catal Today 148(1–2):12–18
2. Yokoyama T, Setoyama T, Fujita N, Nakajima M, Maki T, Fujii K (1992) Novel direct hydrogenation process of aromatic carboxylic acids to the corresponding aldehydes with zirconia catalyst. Appl Catal A 88(2):149–161

3. Bruce L, Mathews JF (1982) The Fischer–Tropsch activity of nickel–zirconia. Appl Catal 4(4):353–369
4. Rezaei M, Alavi SM, Sahebdelfar S, Bai P, Liu X, Yan Z-F (2008) CO_2 reforming of CH_4 over nanocrystalline zirconia-supported nickel catalysts. Appl Catal B 77(3–4):346–354
5. Jung K, Bell A (2002) Effects of zirconia phase on the synthesis of methanol over zirconia-supported copper. Catal Lett 80(1–2):63–68
6. Knauer B, Krohn K (1995) A reinvestigation of the Meerwein–Ponndorf–Verley reduction. A highly efficient variation using zirconium catalysts. Liebigs Annalen 4:677–683
7. Rakshe B, Ramaswamy V, Hegde SG, Vetrivel R, Ramaswamy AV (1997) Crystalline, microporous zirconium silicates with MFI structure. Catal Lett 45(1–2):41–50
8. Rakshe B, Ramaswamy V, Ramaswamy AV (1996) Crystalline, microporous zirconium silicates with MEL structure. J Catal 163(2):501–505
9. Dongare MK, Sabde DP, Shaikh RA, Kamble KR, Hegde SG (1999) Synthesis, characterization and catalytic properties of ZrAPO-5. Catal Today 49(1–3):267–276
10. Zhu Y, Chuah G, Jaenicke S (2003) Al-free Zr–zeolite beta as a regioselective catalyst in the Meerwein–Ponndorf–Verley reaction. Chem Commun 21:2734
11. Anwander R, Gerstberger G, Palm C, Groeger O, Engelhardt G (1998) Enhanced catalytic activity of MCM-41-grafted aluminium isopropoxide in MPV reductions. Chem Commun 17:1811–1812
12. Leyrit P, McGill C, Quignard Fo, Choplin A (1996) A novel heterogeneous molecular catalyst for the Meerwein–Ponndorf–Verley and Oppenauer reactions. J Mol Catal A: Chem 112(3):395–400
13. Quignard F, Graziani O, Choplin A (1999) Group 4 alkyl complexes as precursors of silica anchored molecular catalysts for the reduction of ketones by hydrogen transfer. Appl Catal A 182(1):29–40
14. Morey MS, Stucky GD, Schwarz S, Fröba M (1999) Isomorphic substitution and postsynthesis incorporation of zirconium into MCM-48 mesoporous silica. J Phys Chem B 103(12):2037–2041
15. Ramanathan A, Subramaniam B, Maheswari R, Hanefeld U (2013) Synthesis and characterization of Zirconium incorporated ultra large pore mesoporous silicate, Zr–KIT-6. Microporous Mesoporous Mater 167:207–212
16. Do DM, Jaenicke S, Chuah G-K (2012) Mesoporous Zr-SBA-15 as a green solid acid catalyst for the Prins reaction. Catal Sci Technol 2(7):1417–1424
17. Zhao Z, Liu Y, Wu H, Li X, He M, Wu P (2009) Hydrothermal synthesis of mesoporous zirconosilicate with enhanced textural and catalytic properties with the aid of amphiphilic organosilane. Microporous Mesoporous Mater 123(1–3):324–330
18. Kore R, Srivastava R, Satpati B (2013) Highly efficient nanocrystalline zirconosilicate catalysts for the aminolysis, alcoholysis, and hydroamination reactions. ACS Catal 3(12):2891–2904
19. Chen LH, Xu ST, Li XY, Tian G, Li Y, Rooke JC, Zhu GS, Qiu SL, Wei YX, Yang XY, Liu ZM, Su BL (2012) Multimodal Zr–Silicalite-1 zeolite nanocrystal aggregates with interconnected hierarchically micro–meso–macroporous architecture and enhanced mass transport property. J Colloid Interface Sci 377(1):368–374
20. Kriesel JW, Sander MS, Tilley TD (2001) Block copolymer-assisted synthesis of mesoporous, multicomponent oxides by nonhydrolytic, thermolytic decomposition of molecular precursors in nonpolar media. Chem Mater 13(10):3554–3563
21. Scolan E, Sanchez C (1998) Synthesis and characterization of surface-protected nanocrystalline titania particles. Chem Mater 10(10):3217–3223
22. Yoldas B (1986) Zirconium oxides formed by hydrolytic condensation of alkoxides and parameters that affect their morphology. J Mater Sci 21(3):1080–1086. doi:10.1007/BF01117398
23. Debecker DP, Mutin PH (2012) Non-hydrolytic sol–gel routes to heterogeneous catalysts. Chem Soc Rev 41(9):3624–3650
24. Debecker DP, Hulea V, Mutin PH (2013) Mesoporous mixed oxide catalysts via non-hydrolytic sol–gel: a review. Appl Catal A 451:192–206
25. Andrianainarivelo M, Corriu R, Leclercq D, Mutin PH, Vioux A (1996) Mixed oxides SiO_2–ZrO_2 and SiO_2–TiO_2 by a non-hydrolytic sol–gel route. J Mater Chem 6(10):1665–1671
26. Kaper H, Bouchmella K, Mutin PH, Goettmann F (2012) High-surface-area SiO_2–ZrO_2 mixed oxides as catalysts for the Friedel–Crafts–Type alkylation of arenes with alcohols and tandem cyclopropanation reactions. ChemCatChem 4(11):1813–1818
27. Jansen M, Guenther E (1995) Oxide gels and ceramics prepared by a nonhydrolytic sol–gel process. Chem Mater 7(11):2110–2114
28. Styskalik A, Skoda D, Pinkas J, Mathur S (2012) Non-hydrolytic synthesis of titanosilicate xerogels by acetamide elimination and their use as epoxidation catalysts. J Sol Gel Sci Technol 63(3):463–472
29. Goubeau J, Mundiel RZ (1953) Uber das trichlorsiliciumacetat. Z Anorg Allg Chem 272(1–4):313–326
30. Bradley DC, Thomas IM (1960) 765. Metallo-organic compounds containing metal–nitrogen bonds. Part I. Some dialkylamino-derivatives of titanium and zirconium. J Chem Soc (Resumed):3857–3861. doi:10.1039/JR9600003857
31. Rouquerol J, Rouquerol F, Llewellyn P, Maurin G, Sing KSW (2013) Adsorption by powders and porous solids: principles., Methodology and ApplicationsElsevier Science, London
32. Lowell S, Shields J, Thomas M, Thommes M (2004) Characterization of porous solids and powders: surface area, pore size and density, vol 16., Particle Technology Series, Springer, Netherlands
33. Socrates G (2007) Infrared and raman characteristic group frequencies : tables and charts. John Wiley, West Sussex
34. Su Y-l, Wang J, Liu H-z (2002) FTIR spectroscopic study on effects of temperature and polymer composition on the structural properties of PEO–PPO–PEO block copolymer micelles. Langmuir 18(14):5370–5374
35. Deacon G, Phillips R (1980) Relationships between the carbon–oxygen stretching frequencies of carboxylato complexes and the type of carboxylate coordination. Coord Chem Rev 33(3):227–250
36. Doeuff S, Henry M, Sanchez C, Livage J (1987) Hydrolysis of titanium alkoxides: modification of the molecular precursor by acetic acid. J Non-Cryst Solids 89(1–2):206–216
37. Kongwudthiti S, Praserthdam P, Tanakulrungsank W, Inoue M (2003) The influence of Si–O–Zr bonds on the crystal-growth inhibition of zirconia prepared by the glycothermal method. J Mater Proc Technol 136(1–3):186–189
38. Chen S-G, Yin Y-S, Wang D-P (2005) Formation of ring-like Si–O–Zr bonds at intergranular interfaces in silica-doped zirconia. J Am Ceram Soc 88(4):1041–1045
39. Miller JM, Lakshmi LJ (1998) Spectroscopic characterization of sol–gel-derived mixed oxides. J Phys Chem B 102(34):6465–6470
40. Balmer ML, Bunker BC, Wang LQ, Peden CHF, Su Y (1997) Solid-state 29Si MAS NMR study of titanosilicates. J Phys Chem B 101(45):9170–9179
41. Sindorf DW, Maciel GE (1982) Cross-polarization magic-angle-spinning silicon-29 nuclear magnetic resonance study of silica gel using trimethylsilane bonding as a probe of surface geometry and reactivity. J Phys Chem 86(26):5208–5219
42. Tanabe K (1999) Industrial application of solid acid–base catalysts. Appl Catal A 181(2):399–434
43. Chen S-Y, Lee J-F, Cheng S (2010) Pinacol-type rearrangement catalyzed by Zr-incorporated SBA-15. J Catal 270(1):196–205
44. Ramanathan A, Castro Villalobos MC, Kwakernaak C, Telalovic S, Hanefeld U (2008) Zr-TUD-1: a Lewis acidic, three-

dimensional, mesoporous, zirconium-containing catalyst. Chemistry 14(3):961–972
45. Tanev PT, Pinnavaia TJ (1996) Mesoporous silica molecular sieves prepared by ionic and neutral surfactant templating: a comparison of physical properties. Chem Mater 8(8):2068–2079
46. Yang P, Zhao D, Margolese DI, Chmelka BF, Stucky GD (1999) Block copolymer templating syntheses of mesoporous metal oxides with large ordering lengths and semicrystalline framework. Chem Mater 11(10):2813–2826
47. Barrett EP, Joyner LG, Halenda PP (1951) The determination of pore volume and area distributions in porous substances. I. computations from nitrogen isotherms. J Am Chem Soc 73(1): 373–380
48. Storck S, Bretinger H, Maier WF (1998) Characterization of micro- and mesoporous solids by physisorption methods and pore-size analysis. Appl Catal A 174(1–2):137–146
49. Tanabe K, Misono M, Ono Y, Hattori H (eds) (1989) New solid acids and bases: their catalytic properties. In: Studies in surface science and catalysis, vol 51. Elsevier
50. De bruyn M, Limbourg M, Denayer J, Baron GV, Parvulescu V, Grobet PJ, De Vos DE, Jacobs PA (2003) Mesoporous Zr and Hf catalysts for chemoselective MPV reductions of unsaturated ketones. Appl Catal A 254(2):189–201